

Magnetic Field Measurements in Multi-Beam Deflector Array

W.G. Ras

Magnetic Field Measurements in Multi-Beam Deflector Array

by

W.G. Ras

to obtain the degree of Bachelor of Science
at the Delft University of Technology,
to be defended publicly on Wednesday July 4, 2018 at 10:00 AM.

Student number: 4456572
Project duration: April 23, 2018 – July 6, 2018
Thesis committee: Prof. dr. ir. P. Kruit, TU Delft, thesis supervisor
Dr. ir. J. P. Hoogenboom, TU Delft, 2nd examiner
ir. X. Guo, TU Delft, supervisor
ir. M. A. R. Krielaart, TU Delft, supervisor

This thesis contains patent pending intellectual property (No. USP202772A) and cannot be made public until 09-2019.

An electronic version of this thesis is available at <http://repository.tudelft.nl/>.

Preface

It was a great pleasure to do my bachelor thesis at the Charged Particle Optics research group. The project was very interesting and I have learned a lot about the subject of this thesis but also about doing research in general, so thank you Pieter for the opportunity and thank you Xiaoli for supervising the project. Furthermore, Maurice, you provided knowledge and skills in almost every part of my project. You came up with the some ideas important for the completion of this thesis so I am thankful for that. I also want to thank Ruud for his ever so friendly technical assistance in the realization of the project. Lastly, I want to express my gratitude towards all the others helping me along the way, even in the smallest possible way.

W.G. Ras
Delft, July 2018

Abstract

The Wien filter is an important part in the multi-beam inspection microscope that is being developed at the Imaging Physics research group at the TU Delft. The multi-beam inspection microscope uses an array of 20x20 parallel beams with a pitch of 1 mm that scan the sample simultaneously. This way the low throughput of current scanning electron microscopes can be increased proportional to the number of parallel beams. The Wien filter uses a magnetic field to separate the array of primary beams from the secondary beams. A design for the Wien filter is described in [6] consisting of electric and magnetic deflection arrays. In this report a first model of the magnetic deflection array is presented and tested to investigate the uniformity of the magnetic field. The magnetic field strength was computed by measuring the deflection distance caused by the field. As predicted by theory, the field has been found to scale linearly with the applied current. Current optimization was done in simulations to find the most uniform distribution of the magnetic field. Experiments showed against expectation that the uniformity of the magnetic field between slits does not increase with increasing current on the auxiliary coil while current on the main coil is kept constant. An possible explanation is provided in this report. For the model presented in this report the current in the auxiliary coil should be set to zero in order to obtain the most uniform magnetic field. It is proposed to provide every single winding with its own power supply so that a better uniformity might be achieved by the individual optimization of the currents applied.

Contents

1	Introduction	1
2	Theoretical background	3
2.1	Scanning Electron Microscopy	3
2.1.1	Composition	3
2.1.2	Resolution	4
2.1.3	Bottleneck	4
2.2	Multi-beam inspection microscope	4
2.2.1	Composition	4
2.2.2	Magnetic deflection array and detector Array	5
2.2.3	Magnetic field measurements	5
3	Design and experimental setup	7
3.1	Wien filter requirements	7
3.2	Proof of concept	7
3.3	Design	8
3.4	Experimental setup	8
3.5	Design challenges.	9
4	Magnetic field simulations	11
4.1	Magnetic field uniformity	11
4.2	Current optimization	12
5	Results and discussion	15
5.1	Magnetic field uniformity	15
5.2	Magnetic field linearity	16
5.3	Current optimization	17
6	Conclusion	19
	Bibliography	21



Introduction

In various fields of science and industry, there is an increasing demand for high throughput imaging at the nanometer scale. In the semiconductor industry this could be used to quickly find particles on a patterned wafer or defects in the resist pattern, In biological research rapid cellular processes could be observed in real time or 3D images of tissue could be made. Electron microscopy has made it possible to image at nanometer resolution, already far beyond the limits of light microscopy, yet the relatively long image acquisition time has restricted its applications in many fields. To allow electron microscopy to reach its full potential, multi-beam systems have been developed which can enhance the throughput by several orders of magnitude [2, 7, 9].

The multi-beam inspection microscope that is being developed at the Charged Particle Optics group at the TU Delft uses a single source and multi-column approach. The source and column of an ordinary scanning electron microscope will be modified to individually focus a square array of 20x20 beams onto the sample with a pitch of 1 mm. These primary electron beams interact with the sample and secondary electron beams are emitted opposite to the primary electron beams. The detection system requires the separation of the secondary beams emitted from the primary beams. A Wien filter has been proposed for the purpose of signal separation [6]. The Wien filter uses magnetic fields in combination with electric fields to filter electrons according to their velocities and is used in many different applications [1, 10, 12, 14].

In the application described in this report, the Wien filter deflects the secondary electrons towards the detector while guiding the the primary electrons undisturbed along their initial trajectory. In this thesis, the design of the Wien filter is described and a first model is tested. This first model is a magnetic deflection array for which the uniformity and strength of the magnetic fields are characterized. This thesis will first explain the theoretical background and discuss the design. Subsequently, simulations will be presented and the experimental results discussed.

2

Theoretical background

2.1. Scanning Electron Microscopy

In scanning electron microscopy an electron beam is generated, focused and then scanned across a sample. The electrons undergo various interactions with the material and are then collected by a detector to be analyzed. From this an image is generated. The strength of electron microscopy is its resolution, yet this comes at a cost of a low throughput rate.

2.1.1. Composition

The general composition of a Scanning Electron Microscope (SEM) is shown in figure 2.1. In the vacuum chamber, electrons are extracted at high temperature from the source and accelerated at high voltage. The beam is centered around the optical axis and collimated by the condenser lenses. This is called the primary electron beam. The objective lens focuses the primary beam onto the sample and scanning coils allow the scanning of the beam over the sample. The electrons undergo various interactions with the sample and are then reflected differently. For these different types of reflection different detection systems are used. The reflected electrons can be separated in two main classes. These are Secondary Electrons (SEs) and Backscattered Electrons (BSEs) [4].

SE are electrons emitted from the surface of the sample after having interacted with the electrons of the sample. SEs are characterized by having energies up to 50 eV. From these electrons information on the topography of the sample can be obtained. A positively biased grid attracts these low energy SEs towards the detector [13].

BSEs are electrons reflected from the surface of the sample after having interacted with the nuclei of the sample [4]. The elastic collisions involved create high energy BSEs that can be used to obtain information about the chemical composition of the sample. Having high velocities the BSEs travel opposite to the primary electrons are not attracted towards the SEs detector but are detected by the BSEs detector around the optical axis.

The image displayed by a SEM maps the varying intensity of any of these signals into the image in a position corresponding to the position of the beam on the specimen when the signal was generated [13].

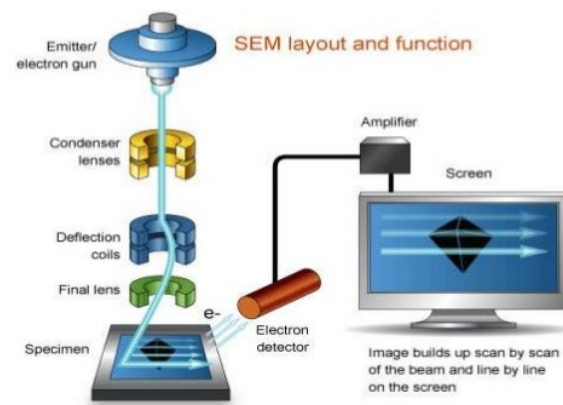


Figure 2.1: The figure shows the general composition of the scanning electron microscope (SEM) for detecting secondary electrons (SE). An electron beam is generated, focused and then scanned across a sample. The electrons interact with the material and are then attracted towards a detector to be analyzed. From this, an intensity image is generated.

2.1.2. Resolution

Electron microscopy revolutionized the way we look at the small things in life. The diffraction limit prohibited optical microscopy from reaching ever higher resolutions [8]. The diffraction limit is seen in formula (2.1) and depends on the wavelength λ and numerical aperture NA . Electron microscopy however achieved sub nanometer resolution by using the wave nature of electrons described by their de Broglie wavelength [3]. Formula (2.2) gives the wavelength λ of an electron with mass m_e and velocity v . Using then the Planck constant h the wavelength of an electron can be calculated that is far smaller than for photons. As an example, an electron with an energy of 30 keV has a wavelength of 0.04 nm, while the wavelength of visible light ranges from 400-700 nm [13].

$$d = \frac{0.61\lambda}{NA} \quad (2.1)$$

$$\lambda = \frac{h}{m_e v} \quad (2.2)$$

2.1.3. Bottleneck

As in any detection system, a certain signal-to-noise ratio (SNR) has to be obtained to create decent images. This means that per position on the sample a sufficient amount of electrons need to be collected. Due to aberrations a SEM can not have a high resolution and a high beam current simultaneously. Thus, with a low current a long dwell time is necessary to get enough signal. This is the bottleneck of electron microscopy. [13]

2.2. Multi-beam inspection microscope

The drawback of scanning electron microscopy is its low throughput [11]. Especially in the semiconductor industry where millions of integrated circuits are patterned on silicon wafers need to be inspected for defects and for particles embedded in the pattern or on top of the wafer. If the wafer of 300 mm in diameter is scanned with a SEM with 10 nm resolution and 100 ns scanning dwell time, it takes 20.000 hours [13]. The electron Optics group at the TU Delft has proposed a multi-beam inspection microscope to increase the throughput time by using multiple beams parallel for scanning the sample surface.[6]

2.2.1. Composition

The technological advances made in the manufacturing of micro-electromechanical systems have made it possible to create aperture arrays used in the single-source, multi-column approach [5] This approach also allows for using the column of an already existing commercial SEM, which already has high quality lenses and high resolution. [13].

Figure 2.2 shows a schematic representation of a multi-beam electron column, At the top of the optical axis the electron source is located. This source generates a diverging electron beam downwards along the optical axis (OA). Multiple primary electron beams are created from this diverging beam by an aperture array. A lens array focuses each primary electron beam at the collimator lens that collimates the beams parallel to the optical axis. The primary electron beams travel along their trajectories through the detector array and Wien filter and are then focused on the sample by the objective lens. Secondary electrons emitted by the sample after interaction with the primary electrons travel up the optical axis, opposite to the primary electrons. At the Wien filter the secondary electrons as separated from the primary electrons by a combination of electric an magnetic fields [6]. This will be explained further in section 2.2.2.

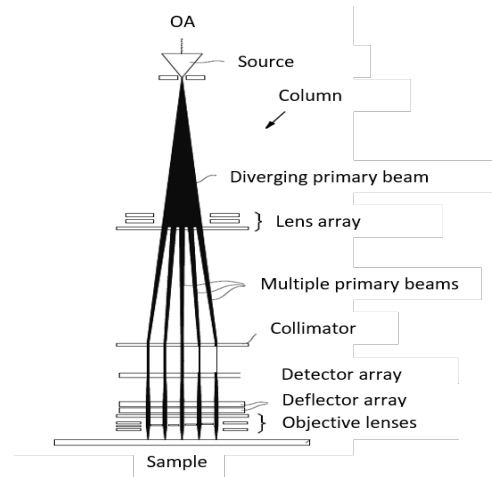


Figure 2.2: General composition of the multi-beam scanning electron microscope where the primary beam from the source is split into an array primary beams and then focused on the sample. [6]

2.2.2. Magnetic deflection array and detector Array

In the multi-beam electron column there is detector array placed in between the collimator and Wien filter, as seen in figure 2.2. The primary electron beams travel along their trajectories through the detector array and Wien filter and are then focused on the sample. More detailed schematics of this part of the column can be seen in figure 2.3.

The detector array is made up from fluorescent strips in combination with an electron-photon converter to generate a signal when electrons hit the surface of the strips. This signal is transported by optical fibers for the image acquisition. This detector array detects secondary electrons emitted by the sample that travel up the optical axis.

The Wien filter consist of magnetic deflection array (MDA) in between two electric deflection arrays (EDA). All arrays consist of a multitude of strips in between which a magnetic or electric field is generated. The electric field is created by applying an potential difference between the different strips. Magnetic fields are generated with use of a coil. Formula 2.3 shows the Lorentz force (\vec{F}_L) working on electrons in a magnetic field (\vec{B}) and electric field (\vec{E}) with the charge and the velocity of the electron represented by q and \vec{v} . The electric and magnetic force are orthogonal to each other. For the Wien filter the forces need to act in the same plane and therefore the strips of the electric deflection arrays are oriented along the x-axis while the strips of the magnetic deflection array are oriented along the y-axis. The combination of the deflection arrays allows the separation of the secondary beams from the primary beams. This is because of the dependence on the velocity vector in the magnetic part of the Lorentz force (\vec{F}_B) as seen in the following formula.

$$\vec{F}_L = \vec{F}_E + \vec{F}_B = q\vec{E} + q(\vec{v} \times \vec{B}) \quad (2.3)$$

Because the secondary electrons have a velocity opposite to the primary electrons the magnetic Lorentz force will thus also be directed in the opposite direction. In figure 2.3 the direction of the the forces due to the magnetic field \vec{F}_B and the electric field \vec{F}_E are represented in blue for the primary electrons and in red for the secondary electrons. In the left of this figure (yz-plane) the primary electrons experience an electric force in the negative y-direction and a magnetic force in the positive y-direction. The fields are tuned so that the first electric field deflects the electrons away from the optical axis. The magnetic field then counteracts this and deflects the electrons back to the optical axis. The second electric field deflects the electrons back along their original trajectory parallel to the optical axis. The primary electrons are focused on the sample by the lenses following the Wien filter. The secondary electrons emitted by the sample travel upwards, opposite to the primary electrons again trough the Wien filter. For the secondary electrons the magnetic force is directed also in the negative y-direction, as are electric forces. The means that the magnetic deflection no longer counteracts the electric deflection but adds to it. The secondary electrons will thus be deflected at an angle from the optical axis so that the they hit the fluorescent strips of the detector array above.

2.2.3. Magnetic field measurements

The aim of this report is to characterize the strength and uniformity of the fields in the magnetic deflector array of the Wien filter. The strength can be obtained by measuring the deflection of the electron beam caused by fields. In this experiment the magnetic deflector array is put into a scanning electron microscope to investigate the fields. In figure 2.4 the schematic overview of the situation is given with the necessary parameters. In formula 2.4 the expression is derived for the deflection angle α caused by an average magnetic field B_{avg} over a distance δ with velocity $\vec{v} = v_z \hat{z}$. What we actually measure is the integral of the magnetic field in the z-direction, but this would be equal to an uniform strength B_{avg} over the height of the slit. The electron mass, charge and momentum in x and y are given by m_e and q and p_x and p_z respectively. The parameters s and h are defined in figure 2.4. Using $\delta = v_z t$ and that \vec{v} and \vec{B} are orthogonal the following expression is derived.

$$\alpha \approx \tan(\alpha) = \frac{d}{h} = \frac{p_x}{p_z} = \frac{\int F_B dt}{p_z} = \frac{q v_z B_{avg} t}{p_z} = \frac{q \delta B}{p_z} \quad (2.4)$$

From the measurements the parameters d , WD , s and the electron energy q are obtained. Using $p_z = \sqrt{2m_e E}$ the average magnetic field B_{avg} is given by

$$B_{avg} = \frac{d\sqrt{2m_e E}}{q\delta h} \quad (2.5)$$

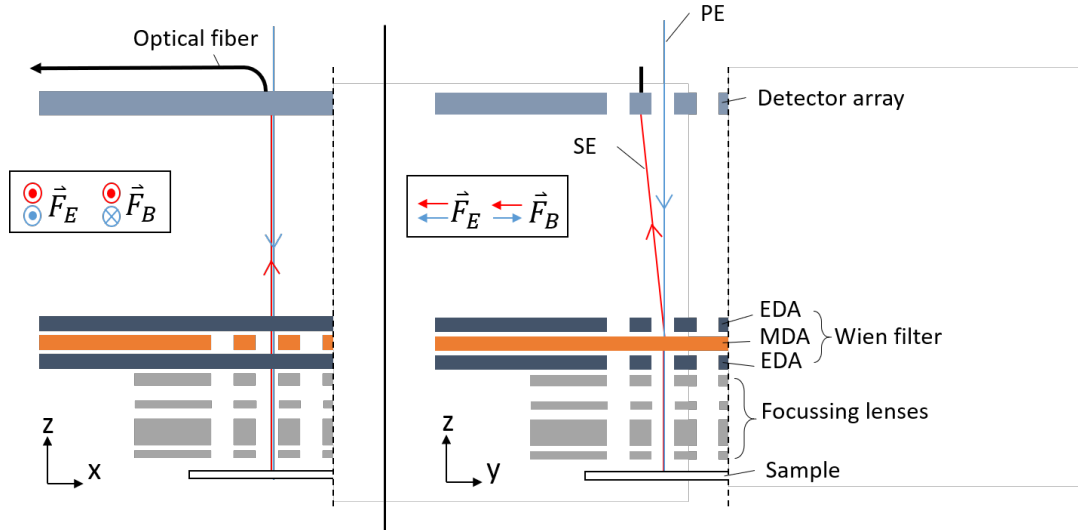


Figure 2.3: Detailed schematics of the detection array and Wien filter [6]. The Wien filter consist of magnetic deflection array (MDA) in between two electric deflection arrays (EDA). All arrays consist of a multitude of strips in between which a magnetic or electric field is generated. The left side of the figure shows the xz -plane and the right side the yz -plane. The primary electrons (PE, blue) experience an electric force \vec{F}_E in the negative y -direction and a magnetic force \vec{F}_B in the positive y -direction. The fields are tuned so that the first electric field deflects the electrons away from the optical axis. The magnetic field then counteracts this and deflects the electrons back to the optical axis. The second electric field deflects the electrons back along their original trajectory parallel to the optical axis. The primary electrons are focused on the sample by the lenses following the Wien filter. The secondary electrons (SE, red) emitted by the sample travel upwards, opposite to the primary electrons again through the Wien filter. For the secondary electrons the magnetic force is directed also in the negative y -direction, as are electric forces. This means that the magnetic deflection no longer counteracts the electric deflection but adds to it. The secondary electrons will thus be deflected at an angle from the optical axis so that they hit the fluorescent strips of the detector array above.

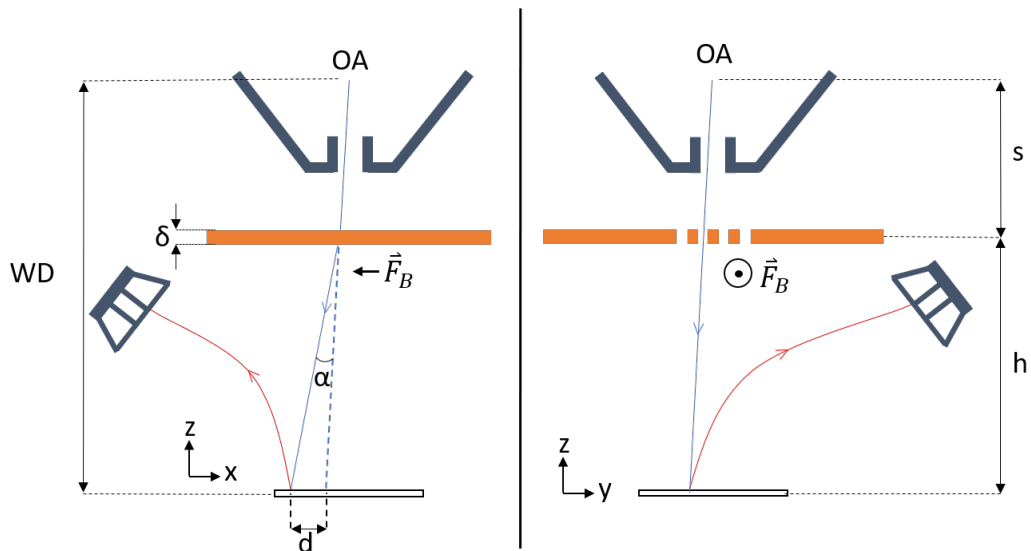


Figure 2.4: The figure gives a schematic overview of the method used to measure the magnetic field strength in the magnetic deflector array. The magnetic deflector array is placed into a SEM and the primary beam (blue) is scanned through the different slits of the array. The secondary beam (SE) is emitted by the sample and attracted towards the detector by a positively biased grid. On the left the xz -plane is shown and on the right the yz -plane. In the measurements an image is generated with zero magnetic field to define the optical axis (OA), then the field is turned on and the deflection d from the optical axis is measured. The angle of the optical axis with the z -axis, or scanning angle, is so insignificant that it can be neglected. With the other parameters shown in the figure, the deflection angle and magnetic field strength can be obtained.

3

Design and experimental setup

In the multi-beam inspection microscope an array of parallel beams are used for imaging. In the previous chapter, it has been explained how the detection system for the multi-beam inspection microscope works. The main elements of the system are the detection array and Wien filter. The Wien filter uses a combination of electric and magnetic fields to deflect secondary electrons towards the fluorescent strips of the detection array. The secondary electrons are converted into photons and are transported by optical fibers for image acquisition. In this chapter the requirements for the Wien filter and the proof of concept. A first model is presented: a magnetic deflection array.

3.1. Wien filter requirements

The requirements for the Wien filter need to be set before explaining the design. There are the following requirements:

Deflection array

The design must deflect an array of at least 20x20 parallel beams with a pitch of 1 mm using a magnetic field.

Uniform magnetic field

It is important that all the beams are deflected equally and no distortions are present. This is necessary because then all the beams are properly detected by the detection array. Equal deflection requires a uniform magnetic field in both dimensions of the array.

High precision alignment

The design must be as such that the array can be aligned at high precision in the column of the multi-beam inspection microscope together with the electric deflector arrays.

3.2. Proof of concept

This thesis presents a first model for the Wien filter for the multi-beam inspection microscope. The following requirements are set for the proof of concept:

Quick implementation

Limited time and means ask for quick and easy implementation of the model. The concept should fit onto an existing stage and in the production materials at hand should be utilized as much as possible.

Proper representation

It is necessary to keep the model as simplistic as possible. Therefore the array should have the minimal number of elements, but still be a proper representation of the 20x20 array. For the model an array of 4x10 elements with a pitch of 1mm is sufficient.

Clear confirmation

The model should be tested using a scanning electron microscope. The results must quantify the magnetic fields in the array. The results must also be comparable with simulations. Furthermore, the model should be as such that it allows the magnetic fields to be adjusted to create a more uniform distribution. Ideally, the field in every slit can be adjusted on its own. For the model a minimum of two different power sources are sufficient.

Scalable

The model should be scalable to a full 20x20 element array with only straightforward adjustments.

3.3. Design

The design and dimensions of the model are shown in figure 3.1. The model consists of an aluminum holder for the mu-metal plate and three mu-metal strips of each 0.5 mm with a gap in between each of also 0.5 mm. This makes 4 slits in total of 25 mm long and with a pitch of 1 mm. Mu-metal has a high relative magnetic permeability (values in the order of $10^4 - 10^5$) and is therefore a good conductor for magnetic field lines, which is expected to benefit the uniformity and field strength in the slits. The value of the relative permeability of the mu-metal used in this model is not known and a conservative value of 10.000 is used in the simulations. Insulated copper wire with a diameter of 0.2 mm is wound four times around the plate at both sides of the gap to make a coil consisting of eight coil generating the main fields. This coil has its own power source. A separate wire is then wound once around every strip and is connected to a different power source. This makes net two coils, one around the plate, from now on called the main coil, and one around the strips, called the auxiliary coil. The main and auxiliary coil have separate power sources making it possible to adjust the magnetic fields in the slit. Note: all the simulation values and measurements in this thesis consider the main coils as single coil. This is because in all the simulations only one winding was used.

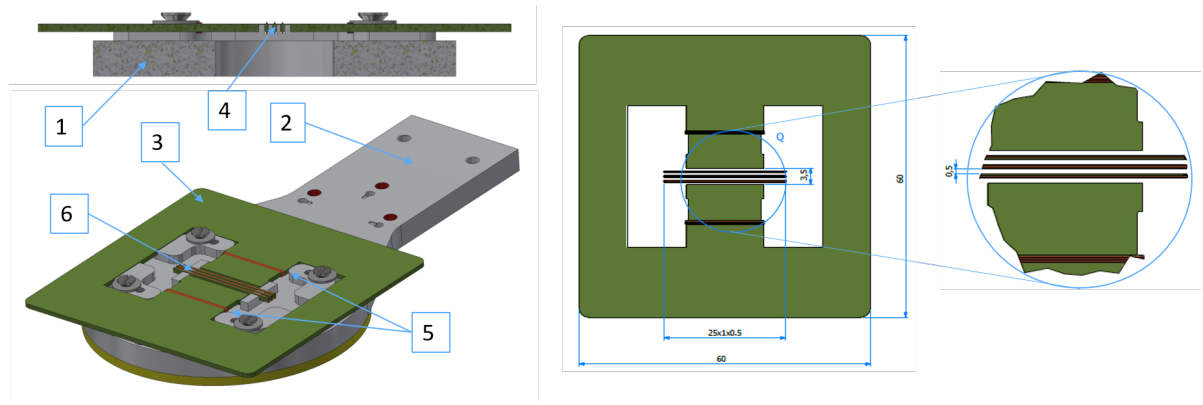


Figure 3.1: The figure shows the design of the model with [1] aluminum holder; [2] racket holder; [3] mu-metal plate; [4] mu-metal strips; [5] main coil; [6] auxiliary coil. The mu-metal strips are longer so that they can be fixed in the aluminum holder and this does not influence the uniformity of magnetic field in the region of interest which is only 10 mm long. The main coils consist of 4 coil each because this was practical. The current of the main coils and auxiliary coil are separately adjustable. Note: all the values and ratios in this thesis consider the main coils as single coil. This is because in all the simulations only one winding was used.

3.4. Experimental setup

The aluminum holder with the plate and strips attached is placed into a racket holder attached to the stage of the microscope. The sample is positioned underneath the deflector array as in figure 2.4. The sample used is a TEM grid. The grid and the measurement procedure are shown in figure 3.3. The stage and the sample can both be translated to adjust the alignment of the optical axis with the various slits and sample. As explained in section 2.2.3 the average magnetic field strength can be computed by measuring the deflection distance caused by that field. The uniformity of the magnetic field is then found by comparing the magnetic field strength for different positions in the slits. The current through the main coils (I_c) and auxiliary coil (I_w) is also varied to see the effect it has on the magnetic field.

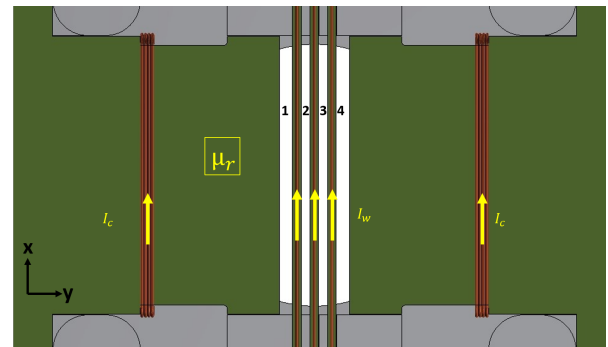


Figure 3.2: The figure shows a close up of the strips and slits. The slits are numbered 1-4 and are used in this way in this report. The current through the main coils I_c is visualized as is the current through the auxiliary coil, I_w . The value for the relative permeability of the mu-metal used in this model is not known and a conservative value of $\mu_r = 10.000$ H/m is used in the simulations. For the air in the slits $\mu_r = 1$ H/m.

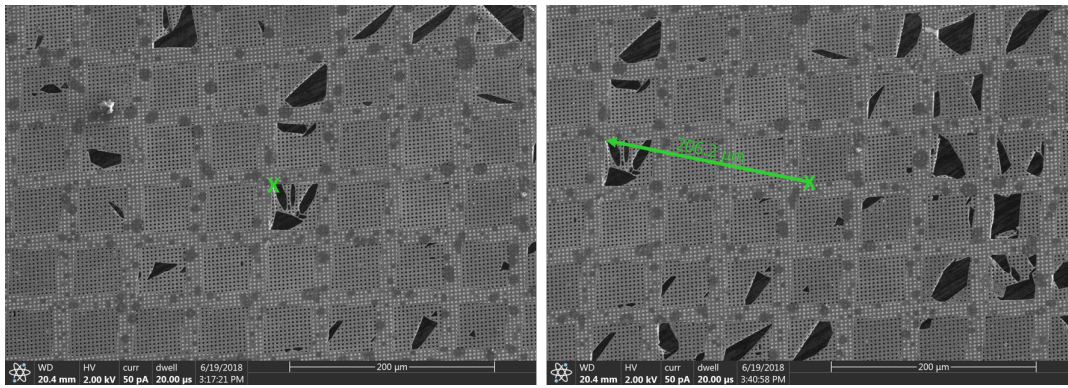


Figure 3.3: The figure shows the sample TEM grid and the measurement procedure in determining the deflection distance. First the optical axis (green X) of the microscope is aligned with a clear feature on the grid when the magnetic field is zero. Then a certain current is applied to the main and auxiliary coil. This translates the image to a new position. In the new image the distance from the optical axis to the feature is measured.

3.5. Design challenges

The design as presented in figure 3.1 creates the following challenges:

Charging

There can not be any insulating material in the field of view of the electron beam. Electrons are not able to flow to ground when landing on insulating material which will cause charging of the material. The charging deflects other electrons from their path decreases the quality of the image generated and must therefore be prevented. The wires are coated with conducting silver paint. An image of the silver coating on the wires is seen in figure 3.4.

Wiring

Another challenge in the assembly process is the winding of the wires, especially around the single strips. A groove was made at both ends of the strips to help stabilizing the wires. The winding must also be done with caution to prevent the sharp edges from breaking through the the insulation of the wire and cause shorts in the circuit.



Figure 3.4: An image by the optical microscope of the auxiliary coil. The wires are coated with conducting silver paint to hide the insulating material from the electron beam.

4

Magnetic field simulations

The first model of the magnetic deflection array has been presented in the previous chapter. It is necessary to get an idea of what to expect in order for the right measurements to be conducted. Specifically, the optimal current on for the main coils (I_c) and auxiliary coil (I_w) can be obtained through simulation. For simplicity the values for the current are represented in ratios ($I_c : I_w$) with $I_c = 50$ mA for all simulations unless explicitly told otherwise. To be clear, 1:0 means that and 1:2 means that $I_c = 50$ mA and $I_c = 100$ mA. All simulations are done COMSOL Multiphysics.

4.1. Magnetic field uniformity

First the the field strength in the different axial directions is simulated for a current ratio of 1:2 and a relative magnetic permeability of $\mu_r = 10.000$ H/m. The results can be seen in figure 4.1. For the x-direction the field seems very uniform for the whole length of the slit. The maximum deviation of field strength is in the order of 1 percent. In the y-direction the strength is observed to decrease going further away from the main coil and closer to the slits. In the outer slits the field strength is significantly higher compared to the inner two slits. The difference is approximately $0.15 \cdot 10^{-4}$ T or 16 percent. The field average of the outer and inner slits is $0.95 \cdot 10^{-4}$ T. For the z-direction the field strength behaves as expected from a deflector. The average field strength that is uniform over the height of the slit is approximately $0.5 \cdot 10^{-4}$ T. The magnetic field strength of the xy-plane at $z=0$ is presented in figure 4.2.

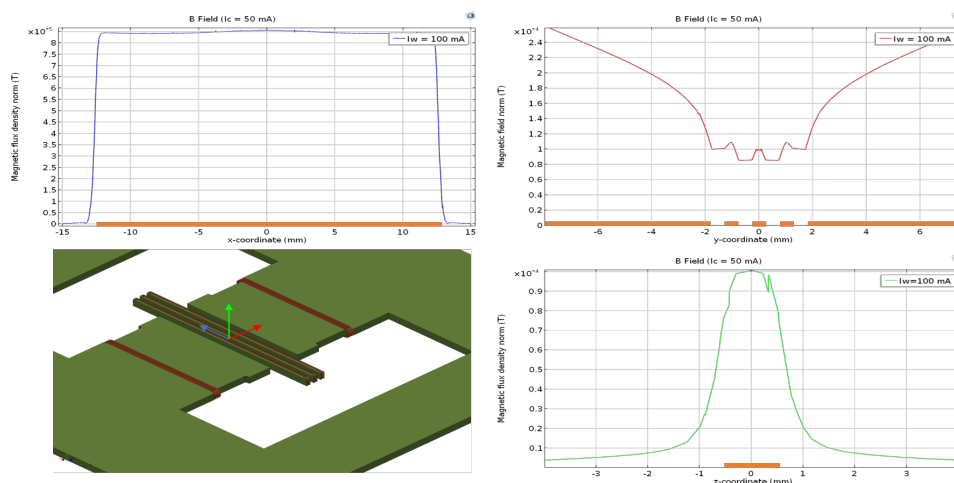


Figure 4.1: This figure shows the the field strength in the different axial directions with current ratio 1:2. The relative permeability of the mu-metal is taken to be 10.000 H/m. (topleft) The magnetic field strength in slit 2 is plotted along the x-direction. The length of the slit is represented by the orange box. (topright) The magnetic field strength plotted along the y-direction over all the slits. The orange boxes represent the plate and slits. (bottomright) The magnetic field strength in slit 2 plotted along the z-direction. The orange box represents the height of the slit. (bottomleft) The orientation of the axes used in the graphs. The colors of the axes match the colors of the corresponding graphs.

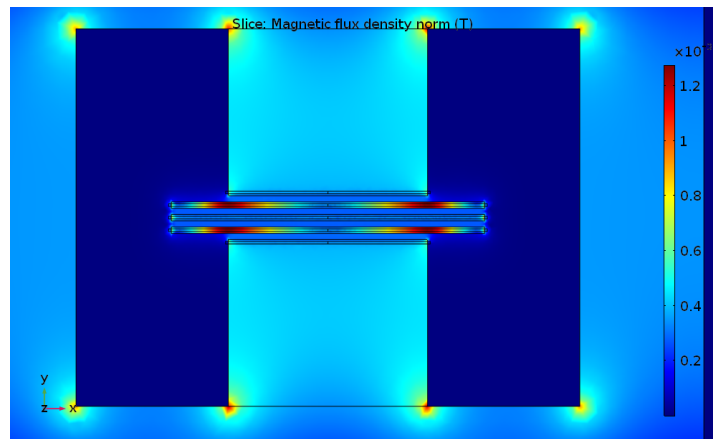


Figure 4.2: Magnetic field strength in the xy-plane at $z=0$ for a current ratio of 1:2. A higher magnetic field strength is seen at the corners of the plate.

For the relative permeability a value of 10.000 H/m was used. This was thought to be a conservative guess of the actual value. It is expected that by increasing the relative permeability for the material the field strength would increase. It is not sure if this also would increase the uniformity of the field. To find the actual value of the relative permeability of the material a parametric study could be done using the experimental results. This is not done investigated in this thesis.

4.2. Current optimization

First the effect of different ratios on the homogeneity of the magnetic field strength is shown. In figure 4.3 the magnetic field strength in the yz-plane is simulated for the ratios 1:1 and 1:2. This effect is further investigated for more current ratios. In figure ?? magnetic field strength is plotted along the y-direction for the current ratios 1:0 up to 1:6 or $I_c = 0..600$ mA. On the left the B-field is plotted, but for to see more clearly the difference in field strength in the slits the H-field is plotted on the right. The H-field outside of materials is equal to the B-field divided by the permeability of the material, the permeability of air $\mu_0 = 4\pi * 10^{-7}$ H/m in this case. One can see that field strength in the outer slits is larger than the inner slits for $I_w = 0$ mA. This difference decreases with increasing current until the most uniform distribution for $I_w = 400$ mA. If the current is increased further the field strength in the inner slits become larger than the outer slits. A current ratio of 1:8 thus seems as the ratio creating the most uniform result with a difference between maximum and minimum of approximately $0.5 * 10^{-5}$ T or 2 percent. This is a significant improvement on the current ratio of 1:2 in figure 4.1. However, while being most uniform overall, the distribution for $I_w = 400$ mA is less horizontal for the inner slits than for example for $I_w = 100$ mA.

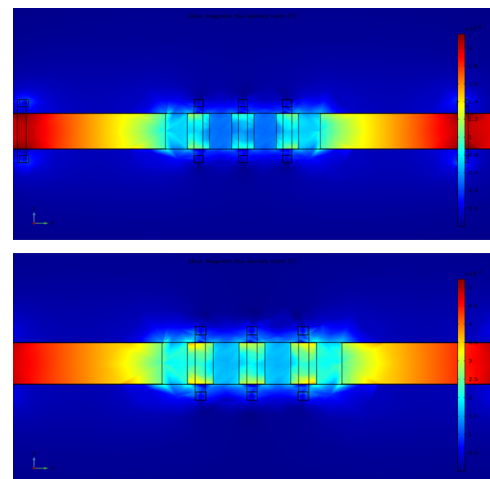


Figure 4.3: (top) The magnetic field strength for a slice of the yz-plane at $x=0$ for a current ratio of 1:1. (bottom) The magnetic field strength for a slice of the yz-plane at $x=0$ for a current ratio of 1:2.

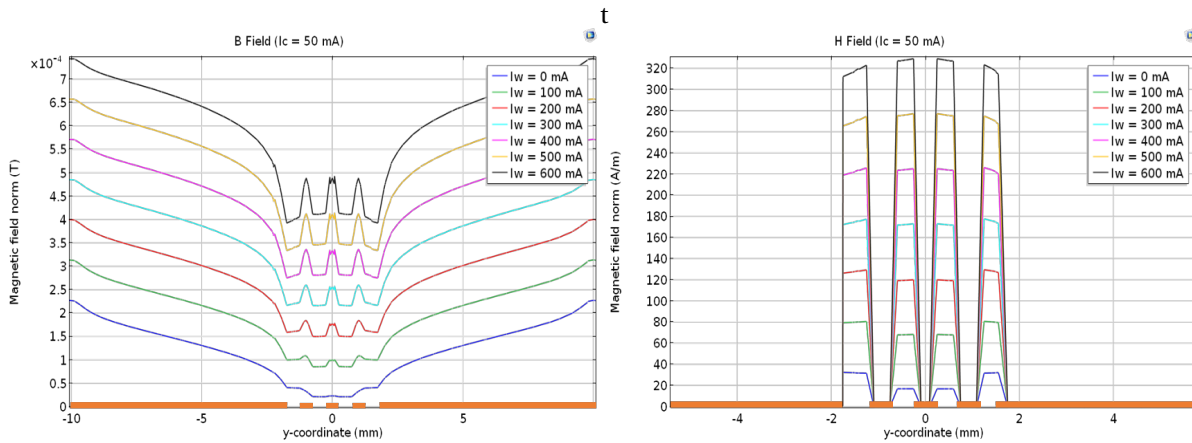


Figure 4.4: This figure shows the B-field (left) and H-field (right) strength for different current ratios. I_c is kept at 50 mA and I_w is increased from 0 to 600 mA. When inspecting this graph, it can be expected that for $I_w = 400$ mA or a current ratio of 1:8 the field is most uniform across all the slits.

One may wonder how this field strength distribution will look like if we increase the number of array elements to a full array of 20x20. Again for various current ratios the H-field is plotted along the y-direction of the array. This is shown on the left in figure 4.5. The most homogeneous distribution seems for $I_w = 700$ mA or a ratio of 1:14. This already indicates that for a different number of array elements there is a different optimal current ratio. For this current ratio a more precise simulation is done and shown on the right of figure 4.5. The field strength is not extremely uniform and still varies for the different slits. The maximal difference in field strength between slits is about $0.25 \cdot 10^{-5}$ T or 3 percent. When these values are compared to the ones calculated for the 3 element array the absolute field strength difference between the slits is lower for the 20 element array with $0.25 \cdot 10^{-5}$ T against $0.5 \cdot 10^{-5}$ T, yet relatively compared to the average field strength in the slits the difference is larger, 3 percent against 2 percent. For the Wien filter only the absolute difference in field strength matters because the deflection in the different slits must be as equal as possible. Thus it looks like that increasing the number of elements increases the uniformity of the magnetic field strength in the slits.

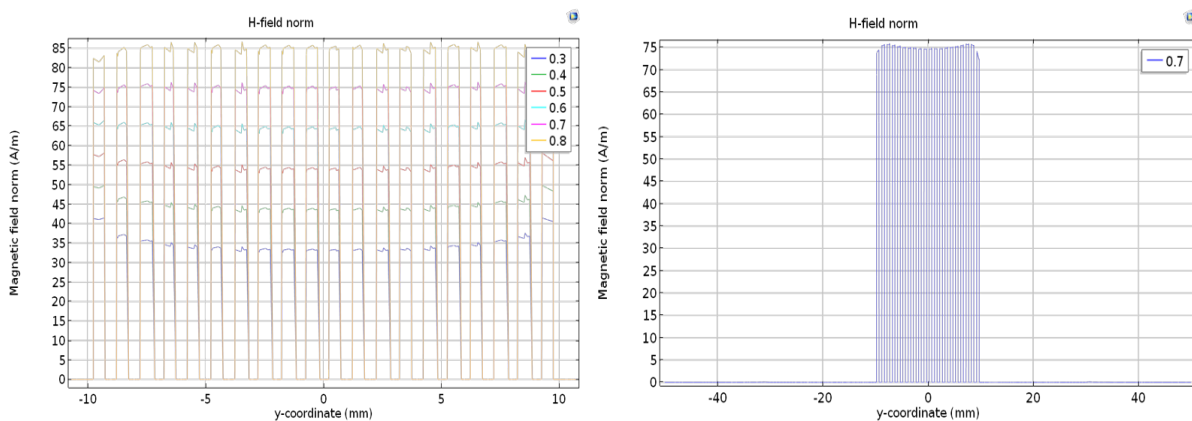


Figure 4.5: (left) The H-field strength simulated for different current ratios. I_c is kept at 50 mA while I_w is increased from 300 mA to 800 mA. The most homogeneous distribution seems for $I_w = 700$ mA or a ratio of 1:14. (right) The simulation on the left seems very crude and therefore in this graph the H-field strength for $I_w = 700$ mA is simulated more precisely. The field strength is not extremely uniform and still varies for the different slits. The maximal difference in field strength between slits is about $0.25 \cdot 10^{-5}$ T or 3 percent.

5

Results and discussion

The measurements described in chapter 3 are now performed. First, the uniformity and linearity of the magnetic field are measured. Uniformity measurements are done for different current ratios to find the optimal value. Magnetic field strength is then compared to the simulations.

5.1. Magnetic field uniformity

As explained in figure 3.3, if current is applied the image will shift due to deflection by the magnetic field in the slits. In figure 5.1 an image is shown from the strips with the sample visible in between. An important question is whether all points in the slit are deflected equally. This has been measured for various points along the length and width of the slit as seen in figure 5.1. In the length of the slit the deflection d due to the applied currents $I_c = 40$ mA and $I_w = 80$ mA was measured along the x-direction about every 2 mm. The average magnetic field strength B_{avg} is also computed. What we actually measure is the integral of the magnetic field in the z-direction, but this would be equal to an uniform strength B_{avg} over the height of the slit. The results are presented in the table 5.1. The length of the slit is 15.9 mm. The average magnetic field is seen to decrease away from the centre of the slit. This is expected through simulation as seen in the upper left graph of figure 4.1. The difference of B_{avg} between the maximum and minimum is 5.6 percent compared to the mean of 0.304 mT. The deflection distance d were also measured at the centre along the width of the slit for positions y . The slit is 0.5 mm wide and about every 0.1 mm the deflection was measured. The applied currents were $I_c = 40$ mA and $I_w = 80$ mA. Again the average magnetic field B_{avg} was computed. The results are shown in 5.2.

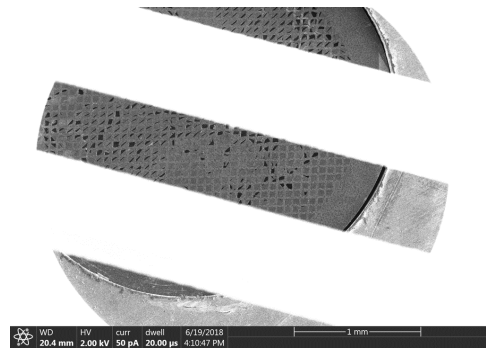


Figure 5.1: Image by the scanning electron microscope of the strips with the sample visible in between.

Table 5.1: The deflection distance d measured along length of the first slit for positions x with applied currents $I_c = 40$ mA and $I_w = 80$ mA. The average magnetic field strength B_{avg} is also computed. The uncertainties for the deflection distances are ± 0.1 μm . The uncertainties in the magnetic field are ± 0.002 mT.

x (mm)	2.50	5.00	7.50	10.0	12.5	15.0
d (μm)	32.8	33.5	34.60	34.0	34.0	34.4
B_{avg} (mT)	0.294	0.301	0.311	0.305	0.305	0.309

Table 5.2: The deflection distance d measured along the width of the first slit for positions y with applied currents $I_c = 40$ mA and $I_w = 80$ mA. At $y = 0$ mm the main plate is located and at $y = 0.5$ mm the first strip. The average magnetic field strength B_{avg} is also computed. The uncertainties for the deflection distances are ± 0.1 μm . The uncertainties in the magnetic field are ± 0.002 mT

y (mm)	0.1	0.2	0.3	0.4
d (μm)	33.9	33.9	33.5	33.2
B_{avg} (mT)	0.304	0.304	0.301	0.298

5.2. Magnetic field linearity

The relation for the magnetic field as a function of deflection as given in formula 2.5 is linear. The first step is to confirm this linearity. In 5.2 the magnetic field strength is computed for an increasing current of the main coils, while the current of the auxiliary coil is set to zero. This measurement is done at the centre and at a quarter of slit 1 and 2. First we see that there is barely any difference in field strength between the centre and the quarter of both slits. Furthermore, we see almost perfect linearity in the magnetic field strength for both slit 1 and slit 2. As expected, there is also a difference in magnetic field strength between the slits. The difference between the slits increases as well with the current. This is only the absolute difference. The relative difference, obtained by dividing by the average field strength, is constant, which is what should be the case with a linearly increasing difference.

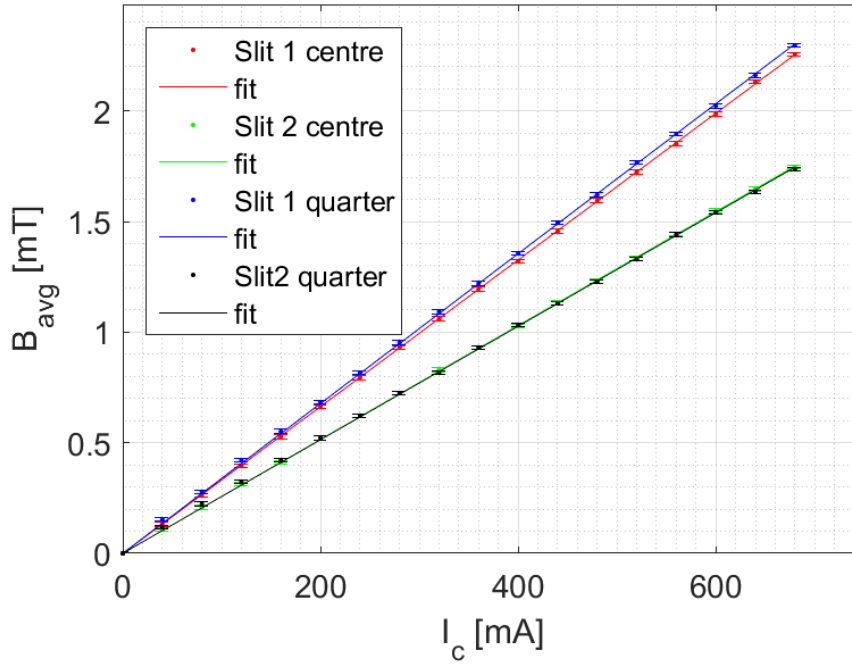


Figure 5.2: Plot of the average magnetic field B_{avg} against the current on the main coils I_c , while the current on the auxiliary coil is zero, $I_w = 0$ mA. Error margins are caused by the uncertainties in using the measuring tool from the software of the SEM.

5.3. Current optimization

As seen in figure 4.4 a current ratio can be found that significantly improves the uniformity of the field strength between the slits. Now measurements are done to confirm if this is the case. This is done by measuring the deflection distance for the outer and inner slit 1 and 2 with the same current ratio in both situations. With the values for the deflection distance in both slits the average magnetic field strength B_{avg} can be computed with formula 2.5. The measurements are done for the ratios of 1:0 up to 1:8 with $I_c = 50$ mA kept constant. There is clearly a difference in the field strength between slit 1 and 2. It is expected from the simulations that the difference between slit 1 and two will decrease with increasing current ratio to an optimal distribution after which it will increase again if the ratio is increased further. Now on the right of figure 5.3 this difference in field strength B_{diff} is plotted.

The figure shows a increasing magnetic field strength difference for an increasing current on the auxiliary coil I_w . This is against the expectations stated before. B_{diff} keeps increasing with I_w thus the uniformity decreases with I_w . The optimal value for I_w is found to be 0 mA, because for this value the difference in field strength between slit 1 and 2 is smallest. Relatively, when the difference between the slits is divided by the average, the difference does decrease for increasing current. This is however not an improvement of the uniformity.

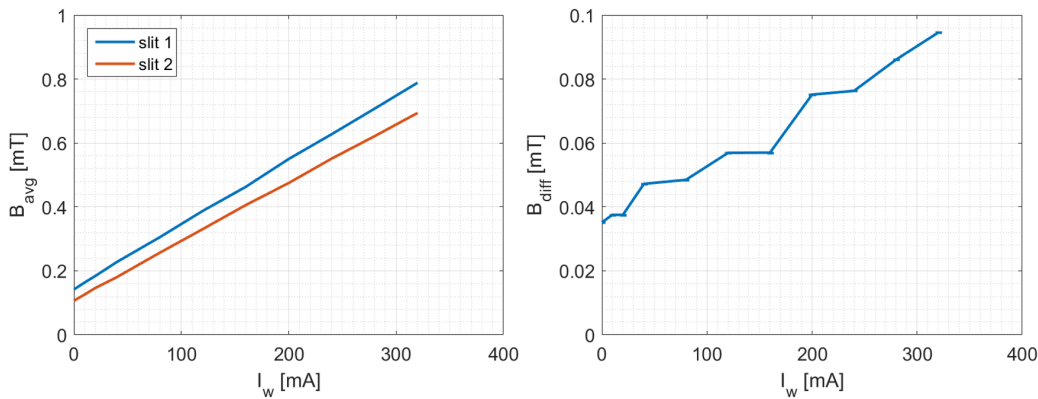


Figure 5.3: (left) Plot of the average magnetic field strength B_{avg} in slit 1 and 2 as a function of I_w . $I_c = 40$ mA and is kept constant throughout the experiment. I_w is increased from 0 mA to 320 mA. This means the ratios 1:0 until 1:8 are measured (while also 2:1 and 4:1 when $I_w = 10$ mA and $I_w = 20$ mA). Error margins are so small they are not visible. (right) Plot of the magnetic field strength difference B_{diff} between slit 1 and 2. The difference increases with increasing current on the auxiliary coil I_w .

Up until now, as in figure 4.4, mainly the field strength along the y-direction have been compared for better uniformity. However, as seen in formula 2.5 the deflection d is dependent on the integral of the field along the z-direction and not only on the strength of the field at $z = 0$ mm. It is therefore investigated how the fields along the z-direction in slit 1 and 2 compare to one another. The magnetic fields along the z-direction in slit 1 and 2 are simulated for the ratio that was measured to be the best (1:0, $I_w = 0$ mA) and for the one expected to be the best from simulations (1:8, $I_w = 400$ mA). These are set alongside the fields in the y-direction that were previously simulated. The result is seen in figure 5.4. By taking a closer look at these figures a possible explanation for the decreasing uniformity is found. It is true that for the ratio 1:8 the field in the y-direction is more uniform, as is $a < b$. This is confirmed by the graph of the field in the z-direction, as in that at $z = 0$ $d < c$. The deflection distance is dependent on the integral of the magnetic field along the z-axis, i.e. the surface beneath the graphs. It looks like the surface between the graphs for slit 1 and 2, $A_1 + A_2$, is greater than the surface, B , for the ratio 1:0. This means that the deflection will be greater for the ratio 1:8. This is a possible explanation for keep increasing field difference as seen in figure 5.3. Figure 5.5 gives further insight on the field in the z-direction for the two current ratios. In this figure a vector plot of the H-field is shown for the yz-plane for the ratio of 1:0 (left) and 1:1 (right). Note that the vectors are normalized for better representation and are thus not proportional to the field strength. It is observed that for the ratio of 1:0 the field above and beneath the strips is more similar than for the ratio of 1:1 where the field lines are curved from one strip to the next. This is cause by applying current on the auxiliary coil. This might be the cause of a relatively higher field strength above and beneath slit 2 for the ratio 1:8 compared to the ratio 1:0.

These are all qualitative observations, to confirm the proposed explanation the integral of the fields along the z-direction need to be computed. This has yet to be done in further research.

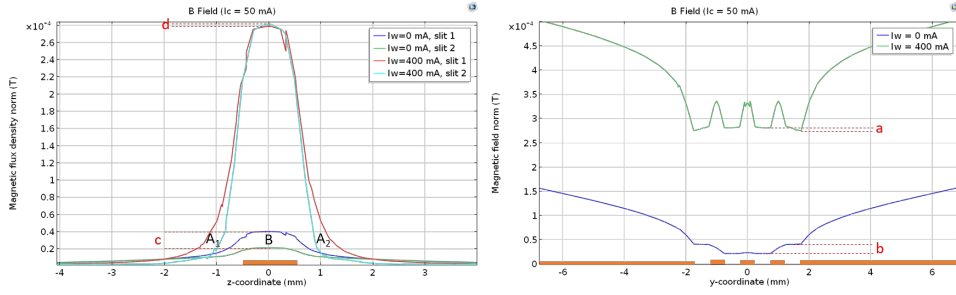


Figure 5.4: (left) The difference in the magnetic field plotted along the z-direction for slit 1 and 2. This is done for the ratio measured to be the best (1:0, $I_w = 0$ mA) and the one expected to be the best from simulations (1:8, $I_w = 400$ mA). The orange box represents the height of the strips. (right) The field plotted for the same ratios 1:0 and 1:8 along the y-direction. The orange box represent the plate and strips of the deflector array.

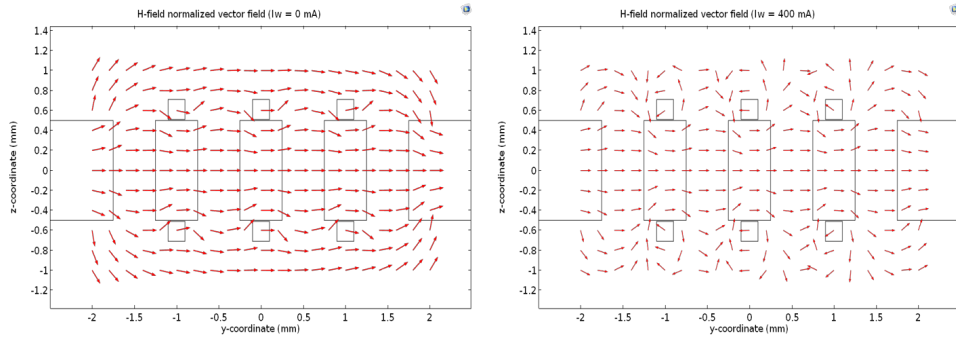


Figure 5.5: In this figure a vector plot of the H-field is given for the yz-plane for the ratio of 1:0 (left) and 1:1 (right) with $I_c = 50$ mA. The vectors are normalized for better representation and are thus not proportional to the field strength.

If the auxiliary coil are not beneficial for the uniformity of the magnetic field in the deflector array, the question is raised whether the mu-metal strips do benefit this. To investigate this the exact same model was simulated only without the strips and auxiliary coil. The result is seen in figure 5.6. It is seen that the field strength is higher in the slits when the strips are present than when the strips are not present. The strength is also more uniform in the slits when the strips are present compared to the parabolic shape of the field strength when no strips are present. It can therefore be concluded that the strips do benefit the magnetic field strength and its uniformity.

Another possibility for explaining 5.3 is an error in the design of the proof of concept. By accident the outer slits have been made $750\mu\text{m}$ wide instead of $500\mu\text{m}$. This does perhaps explain a different deflection than expected, however this effect would be equal for all current ratios and therefore is an unlikely explanation.

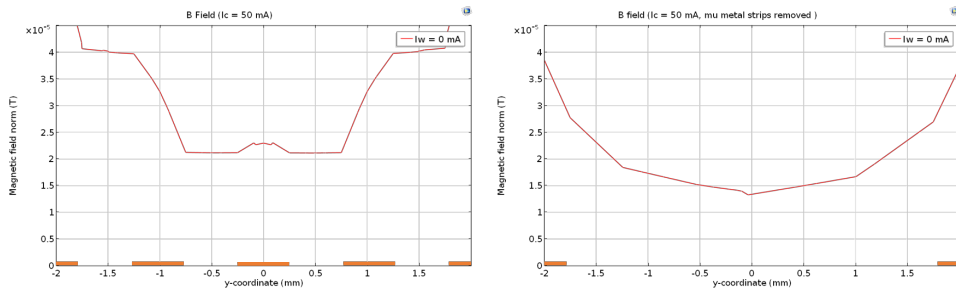


Figure 5.6: Left: The magnetic field strength plotted along the y-direction for a current ratio of 1:0 as seen before. Right: The magnetic field strength plotted along the y-direction for the same model as on the left only with the mu-metal strips removed. The orange boxes represent the plate and strips of the model.

6

Conclusion

The Wien filter is an important part in the multi-beam inspection microscope that is being developed at the Imaging Physics research group at the TU Delft. The multi-beam inspection microscope uses an array of 20x20 parallel beams with a pitch of 1 mm that scan the sample simultaneously. This way the low throughput of current scanning electron microscopes can be increased proportional to the number of parallel beams. The Wien filter uses a magnetic field to separate the array of primary beams from the secondary beams. It is important that all beams experience an equally strong magnetic field in order to deflect all the beams towards the detector. A design for the Wien filter is described in [6] consisting of electric and magnetic deflection arrays. In this report a first model of the magnetic deflection array is presented and tested to investigate the uniformity of the magnetic field. The model is a mu-metal plate consisting of 4 slits with a pitch of 1 mm, creating an proper 4x10 representation of the full 20x20 array. Coils wound around the plate are used to create a magnetic field in between array. A auxiliary coil with a separate power supply is wound around the strips to possibly increase the uniformity of the field. An optimal value for the two currents is expected to be found for which the magnetic field is most uniform.

Various simulations were done to investigate the effect of the applied current on the strength and uniformity of the magnetic field. An optimal value for the current through the auxiliary coil was found to be 8 times the current through the main coil. Simulations done for a 20x20 model found an optimal value of 14 times the current through the main coil. Even with most most optimal values the field was not perfectly uniform and showed slight differences in field strength between the slits.

The magnetic deflector array was also placed into a scanning electron microscope to experimentally investigate its field strength and uniformity. The silver paint used to prevent charging of the insulation of the wire proved successful. An expression was derived for the magnetic field strength as a function of the deflection distance of the electron beam. Experiment were done measuring the deflection of the beam in order to compute the magnetic field strength. It is found that the magnetic field in the deflector array increases linearly with the current applied, as expected from the expression derived. No deformations are seen in the displaced images either. This makes it possible to obtain any magnetic field strength as long as the wires can handle the current. The field strength slightly decreased away from the centre of the slit according to simulations. It was also found that the difference in field strength between slits increased with increasing current on the auxiliary coil while the current on the main coil was kept constant. Thus the uniformity of the field does not improve by applying a current on the auxiliary coil and it is concluded that for this model no current must be applied on the auxiliary coil in order to create the most uniform magnetic field. An possible explanation for this was found when investigating the magnetic field above and beneath the slits. The total deflection depends on the integral of the field along the trajectory of the electrons and this seemed to be greater for higher current applied on the auxiliary coils. Further research needs to be done to prove if the solution proposed in correct. The mu-metal strips do improve the magnetic field strength and the uniformity of the field. It is proposed to provide every single winding around the strips with its own power supply so that a better uniformity might be achieved by the individual optimization of the currents applied.

Bibliography

- [1] W Aberth and H Wollnik. The wien filter and its application in chemistry. *Mass Spectrometry Reviews*, 9 (4):383–404, 1990.
- [2] Pavel Adamec, Ralf Degenhardt, Hans-Peter Feuerbaum, Harry Munack, and Dieter Winkler. Multi beam charged particle device, September 13 2005. US Patent 6,943,349.
- [3] Louis De Broglie. The wave nature of the electron. *Nobel lecture*, 12:244–256, 1929.
- [4] David C Joy. Beam interactions, contrast and resolution in the sem. *Journal of Microscopy*, 136(2):241–258, 1984.
- [5] Jack W Judy. Microelectromechanical systems (mems): fabrication, design and applications. *Smart materials and Structures*, 10(6):1115, 2001.
- [6] P Kruit. Signal separator for a multi-beam charged particle inspection device, 2018. US Patent 202772A.
- [7] Pieter Kruit and Aernout Christiaan Zonneville. Multiple beam charged particle optical system, October 23 2012. US Patent 8,294,117.
- [8] Shinji Okazaki. Resolution limits of optical lithography. *Journal of Vacuum Science & Technology B: Microelectronics and Nanometer Structures Processing, Measurement, and Phenomena*, 9(6):2829–2833, 1991.
- [9] N William Parker, Alan D Brodie, George Xinsheng Guo, Edward M Yin, and Michael C Matter. Electron optics for multi-beam electron beam lithography tool, September 9 2003. US Patent 6,617,587.
- [10] Norman W Parker. Wien filter design, December 6 1988. US Patent 4,789,787.
- [11] RFW Pease and WC Nixon. High resolution scanning electron microscopy. *Journal of Scientific Instruments*, 42(2):81, 1965.
- [12] E Plies, K Marianowski, and T Ohnweiler. The wien filter: History, fundamentals and modern applications. *Nuclear Instruments and Methods in Physics Research Section A: Accelerators, Spectrometers, Detectors and Associated Equipment*, 645(1):7–11, 2011.
- [13] Y Ren. Imaging systems in the delft multi-beam scanning electron microscope 1. *TU Delft repository*, doi:10.4233/uuid:e25ff43d-b8ae-4b6c-9bc9-d10768c4ab11, 2017.
- [14] H Rose. The retarding wien filter as a high resolution imaging filter. *Optik*, 77:26–34, 1987.